The development of cobalt phosphide co-catalysts on BiVO4 photoanodes to improve H2O2 production

Yuntao Xu, Yanfei Cao, Li Tan, Qiao Chen, Yuanxing Fang

Publication date
01-05-2023

Document Version
Accepted version

Published in
Journal of Colloid and Interface Science

Link to external publisher version
https://doi.org/10.1016/j.jcis.2022.11.120

Supporting Information

The development of cobalt phosphide co-catalyst on $BiVO_4$ photoanode to improve H_2O_2 production

Yuntao Xu, [1] Yanfei Cao, [1] Li Tan,[1*] Qiao Chen[2] and Yuanxing Fang[1*]

[1]State Key Laboratory of Photocatalysis on Energy and Environment, College of Chemistry, Fuzhou University, Fuzhou 350116, P. R. China

[2]Department of Chemistry, School of Life Sciences, University of Sussex, Brighton, BN1 9QJ, United Kingdom

Email: tan@fzu.edu.cn; yxfang@fzu.edu.cn.

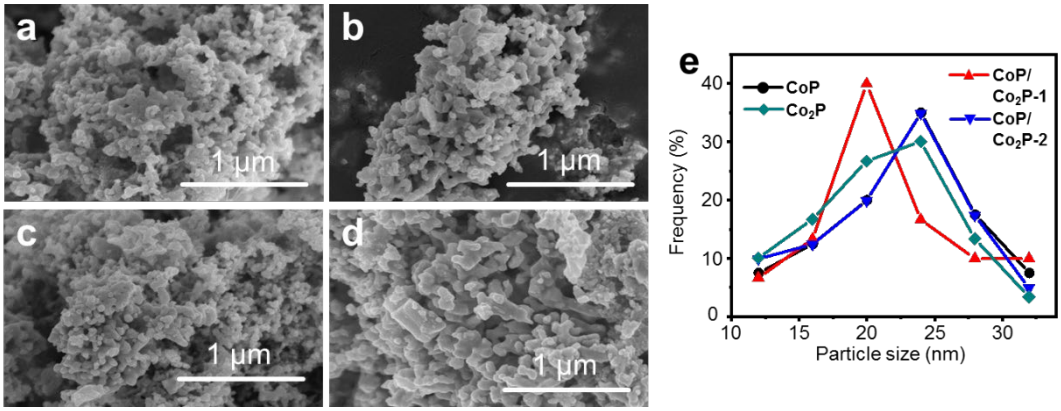

Figure S1. SEM images of (a) CoP, (b) CoP/Co_2P-1, (c) CoP/Co_2P-2 and (d) Co_2P. (e) Particle size distribution of CoP, CoP/Co_2P-1, CoP/Co_2P-2 and Co_2P.

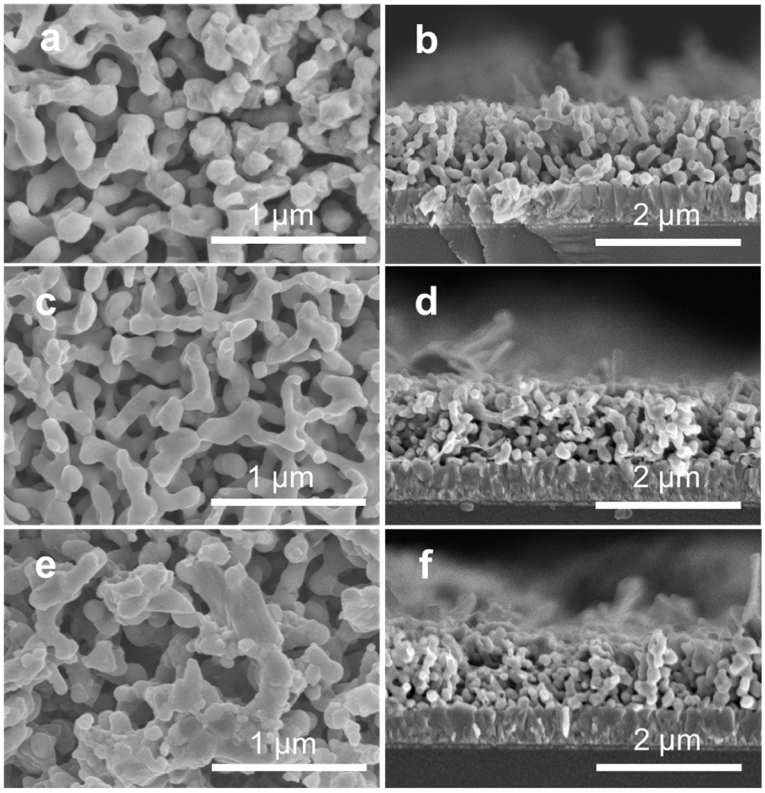

Figure S2. Top view and cross section view SEM images of (a)-(b) CPB-1, (c)-(d) CPB-2 and (e)-(f) CPB-3.

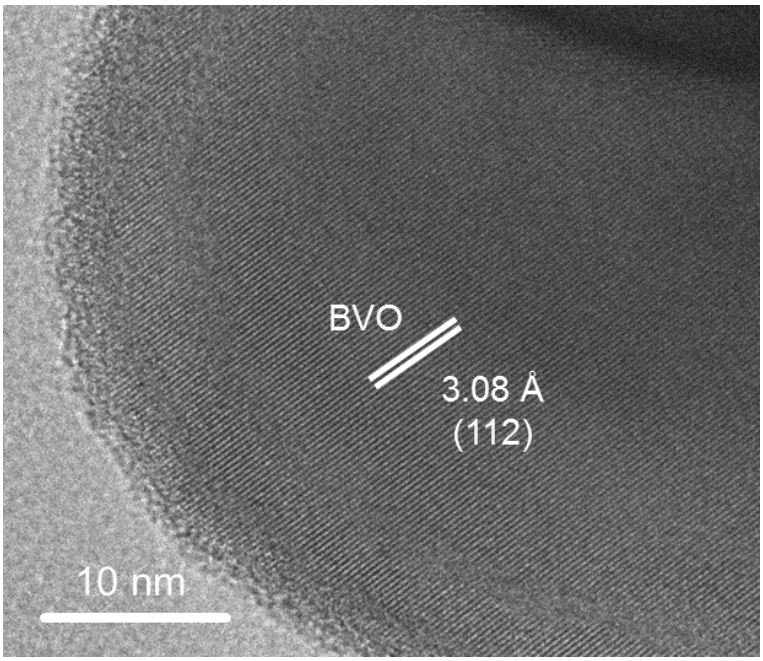

Figure S3. HR-TEM images of pristine BVO photoanode.

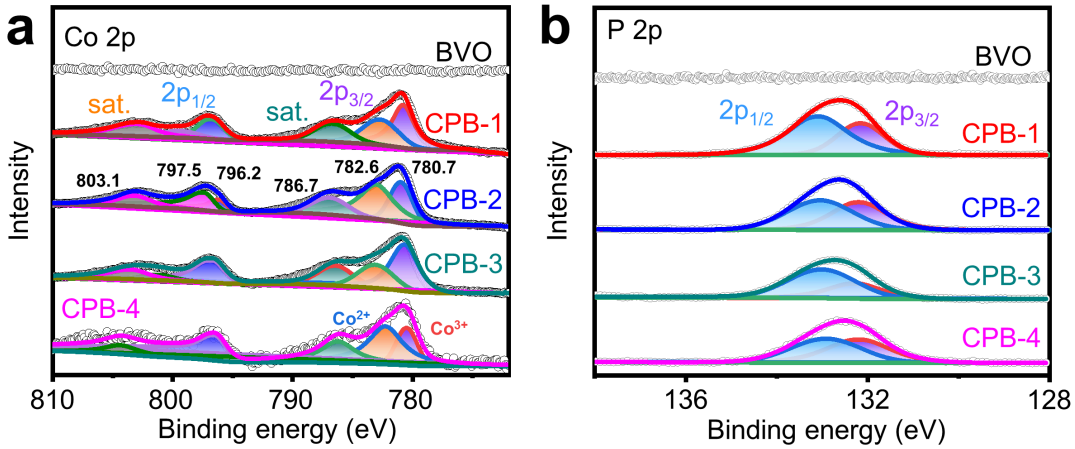

Figure S4. High resolution XPS spectra of (a) Co 2p and (b) P 2p of BVO and CPB photoanodes.

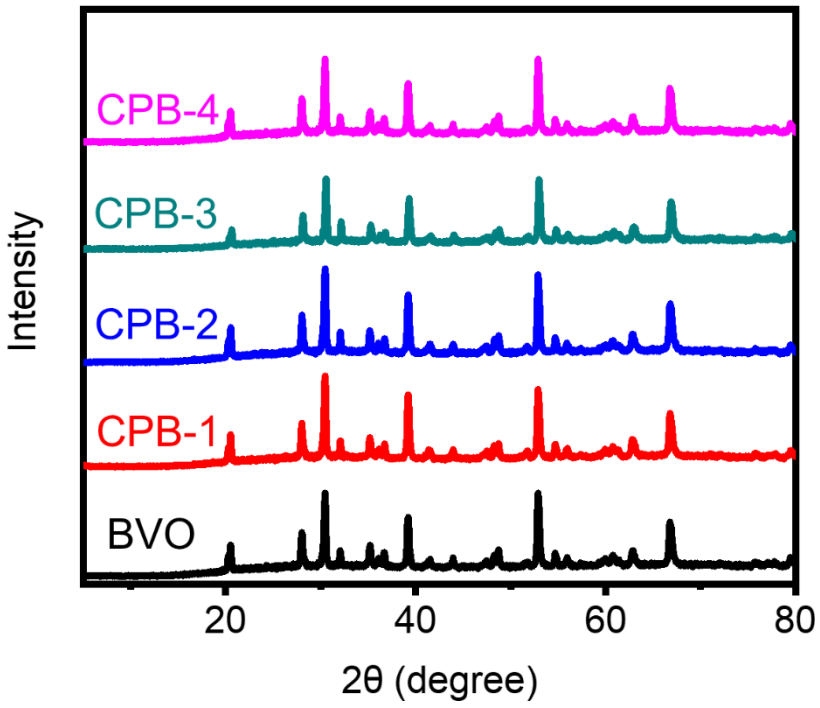

Figure S5. XRD patterns of BVO and CPB photoanodes.

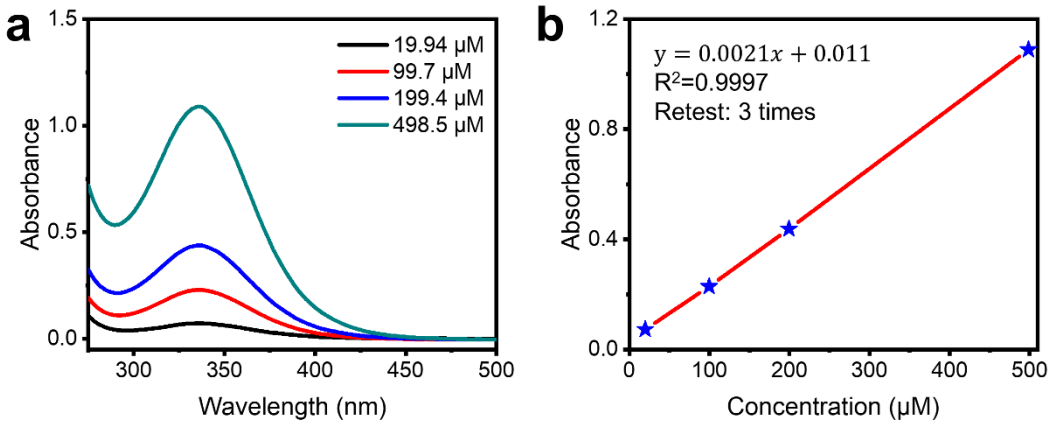

Figure S6. (a) Absorbance curve of standard concentration obtained by UV-Vis-NIR spectrophotometer, (b) the standard curve.

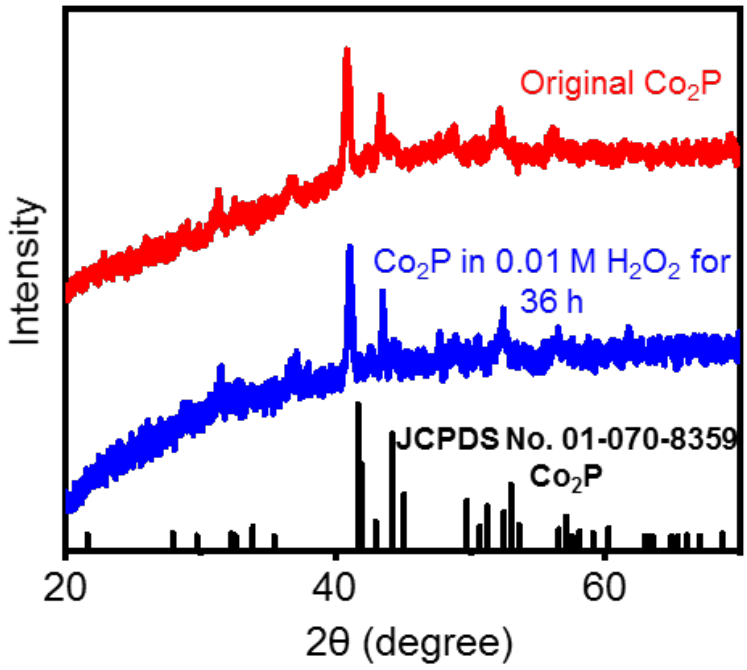

Figure S7. XRD spectra of origin Co_2P and the Co_2P that soaked in 0.01 M H_2O_2 solution for 36 h.

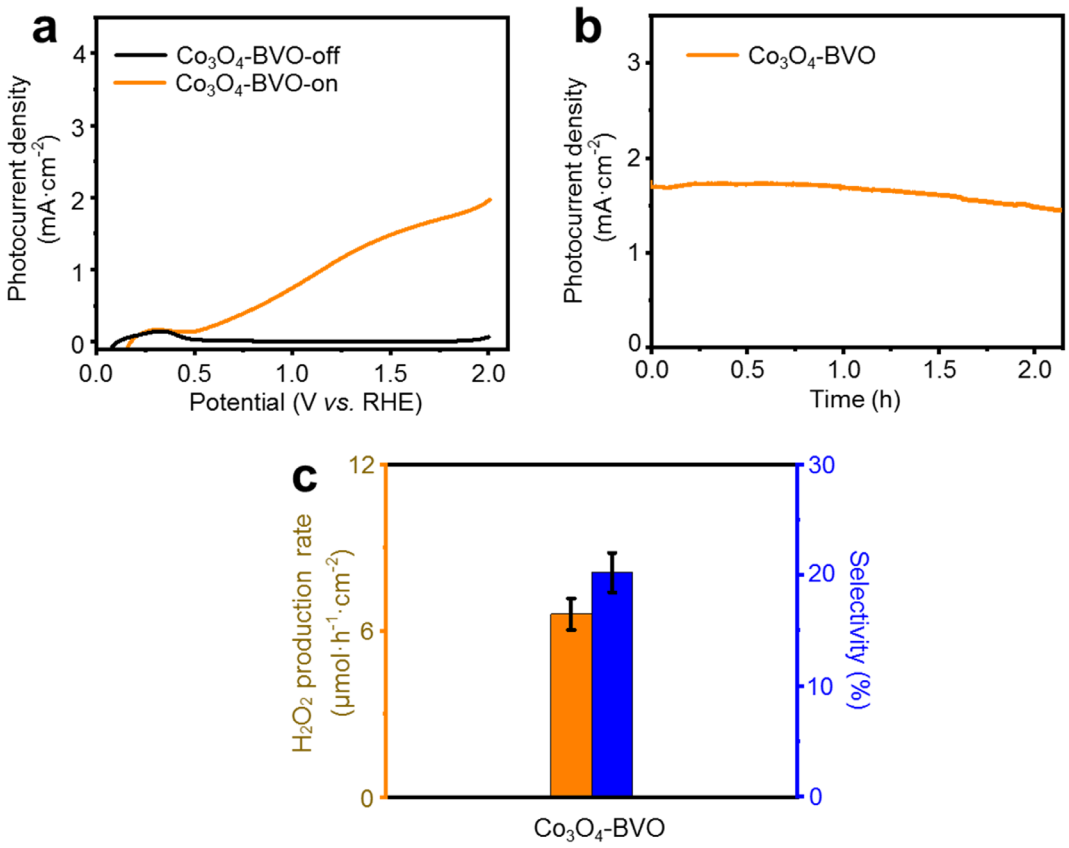

Figure S8. (a) Photocurrent density of the Co_3O_4-BVO photoanode for H_2O_2 production under AM 1.5 G illumination. (b) CA curve of the Co_3O_4-BVO photoanode for H_2O_2 production with the applied voltage of 1.7 V_{RHE}. (c) The H_2O_2 production and selectivity of the Co_3O_4-BVO photoanode for H_2O_2 production with three times of independent repeated experiments.

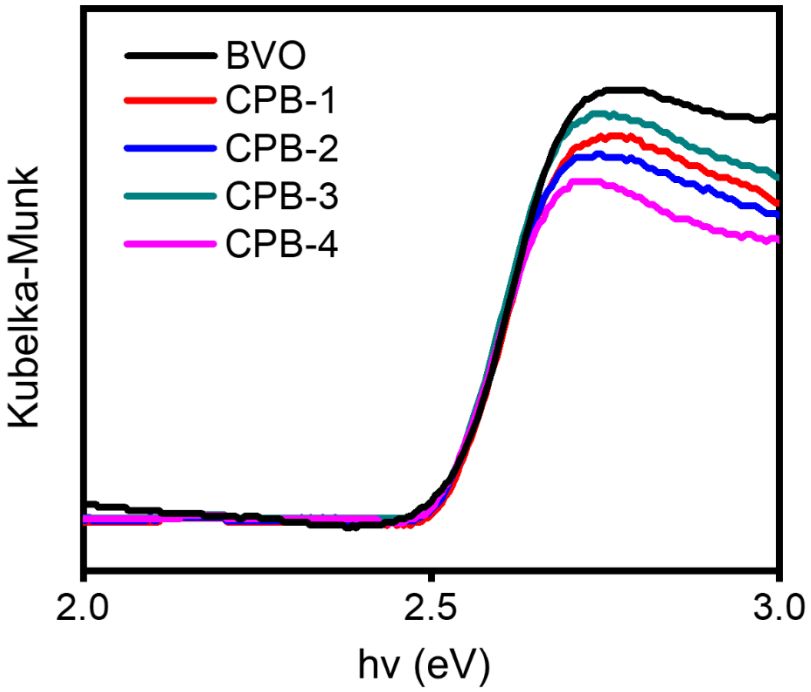

Figure S9. UV-Vis DRS spectra of BVO and CPB photoanodes of Kubelka-Munk spectra.

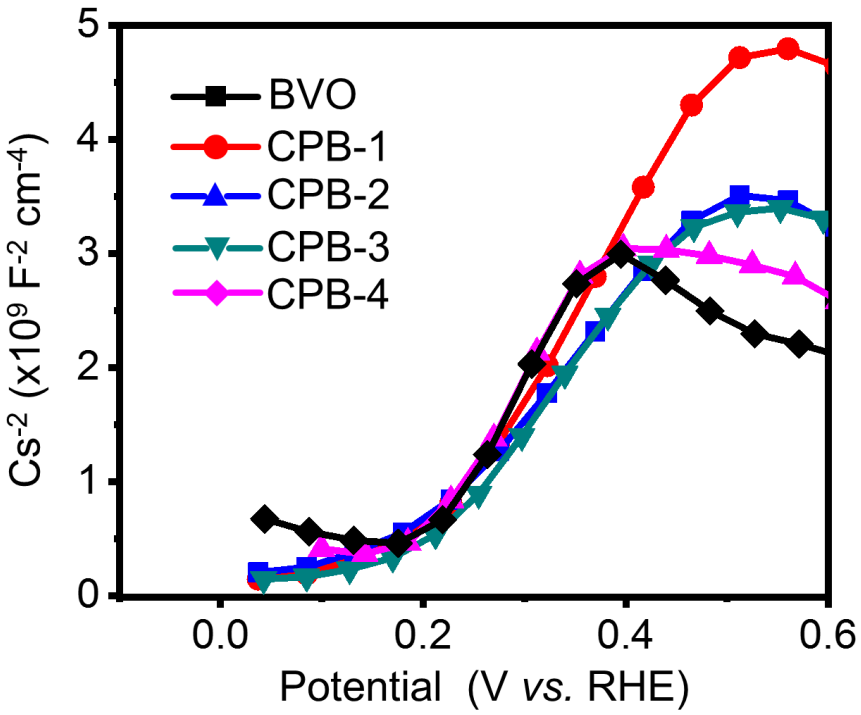

Figure S10. The Mott-Schottky plots to measure the flat-band potentials of BVO photoanode and CPB samples.

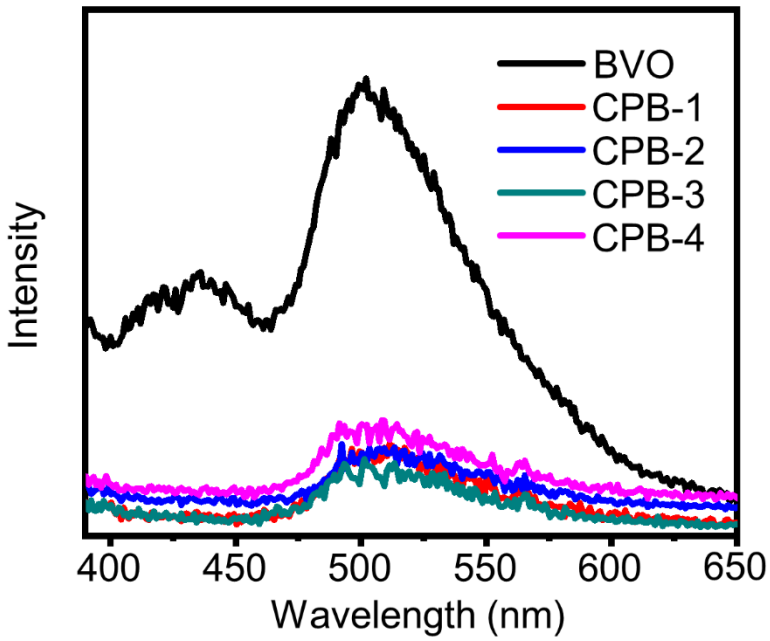

Figure S11. Fluorescence intensity spectra of BVO photoanode and CPB samples.

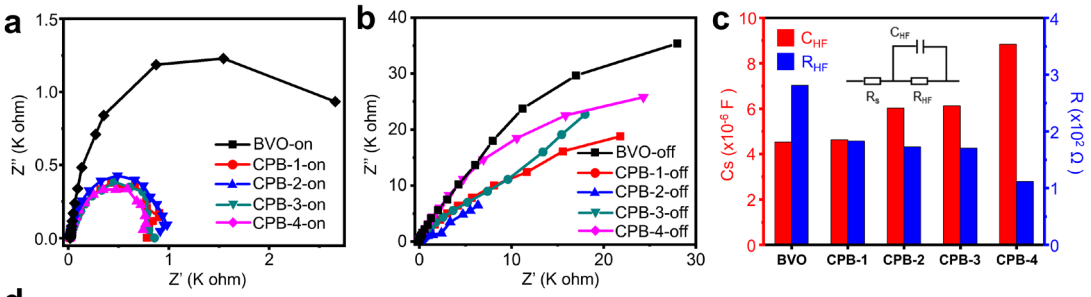

d

Samples	R_s (Ω)	R_{LF} (Ω)	C_{HF} (F)	R_{HF} (Ω)	C_{LF} (F)
BVO	17.11	2850	4.54×10^{-6}	281.2	2.02×10^{-6}
CPB-1	16.56	703	4.62×10^{-6}	183.4	3.48×10^{-6}
CPB-2	17.18	743.1	6.04×10^{-6}	172.9	6.55×10^{-6}
CPB-3	17.26	650.4	6.13×10^{-6}	170.5	7.82×10^{-6}
CPB-4	16.88	587.6	8.84×10^{-6}	112.1	1.70×10^{-5}

Figure S12. The Nyquist plots of EIS measurements of BVO and CPB photoanodes of (a) under illumination, (b) in the dark, with (c) the fitting of the impedance spectrum of R_{HF} and C_{HF}.

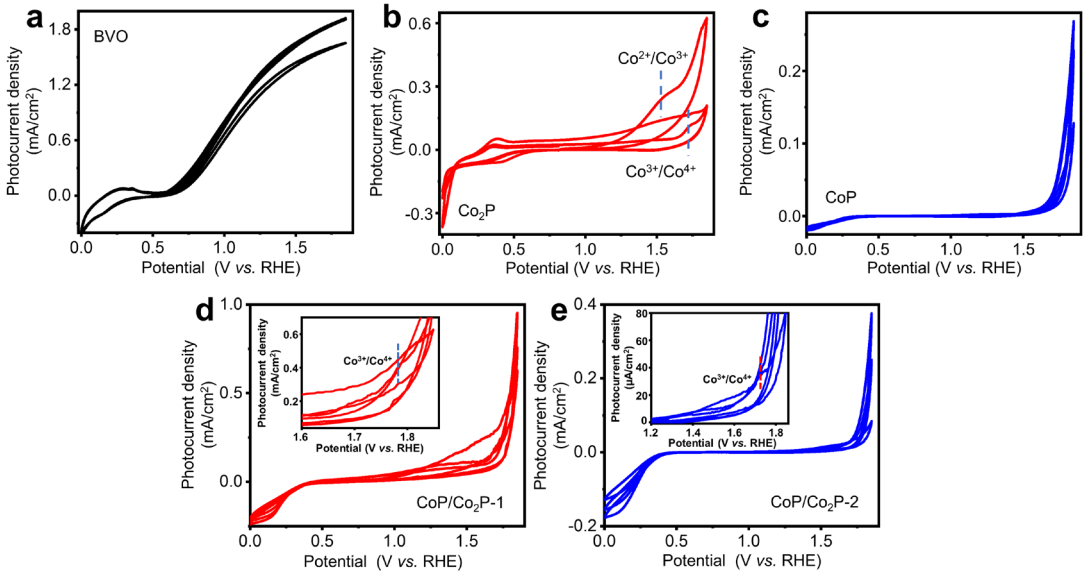

Figure S13. CV curves of (a) BVO, (b) Co_2P, (c) CoP, (d) CoP/Co_2P-1 and (e) CoP/Co_2P-2.

In **Figure S13a**, no apparent peaks can be observed for BVO photoanode at 1.0 to 1.9 V *vs.* RHE. In **Figure S13d** and **13e**, CoP/Co_2P-1 and CoP/Co_2P-2 presented peaks at 1.53 and 1.75 V_{RHE}, which are known as Co^{2+} to Co^{3+} and peaks of Co^{3+} to Co^{4+}.

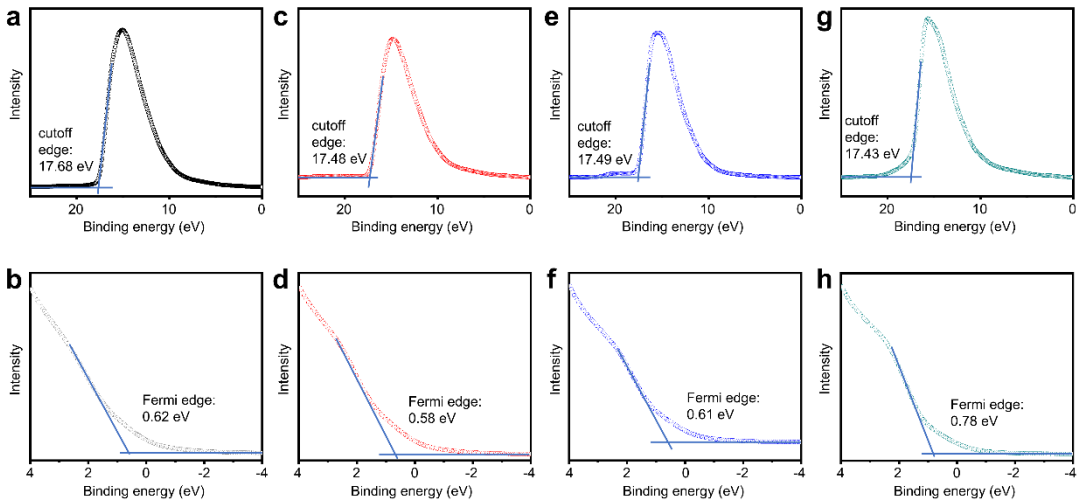

Figure S14. UPS spectra that show the cutoff edge and fermi edge of (a)-(b) CPB-1, (c)-(d) CPB-2, (e)-(f) CPB-3 and (g)-(h) CPB-4.

The cutoff edge of CPB-1, CPB-2, CPB-3 and CPB-4 are 17.68, 17.48, 17.49 and 17.43 eV (**Figure S14a, S14c, S14e,** and **S14g**). The fermi level of CPB-1, CPB-2, CPB-3 and CPB-4 are 0.62, 0.58, 0.61 and 0.78 eV (**Figure S14b, S14d, S14f,** and **S14h**).

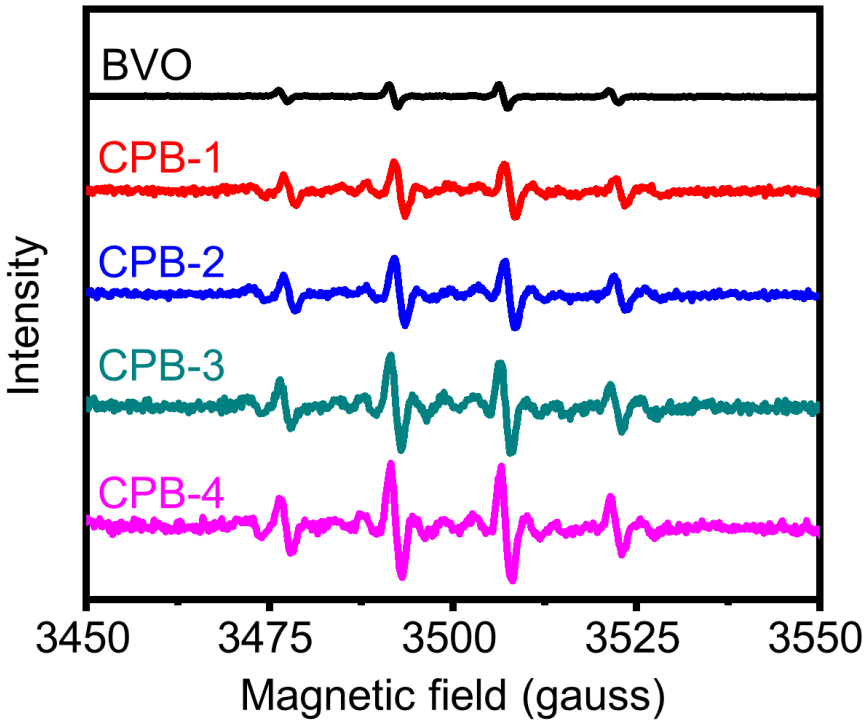

Figure S15. EPR spectra of BVO and CPB photoanodes.

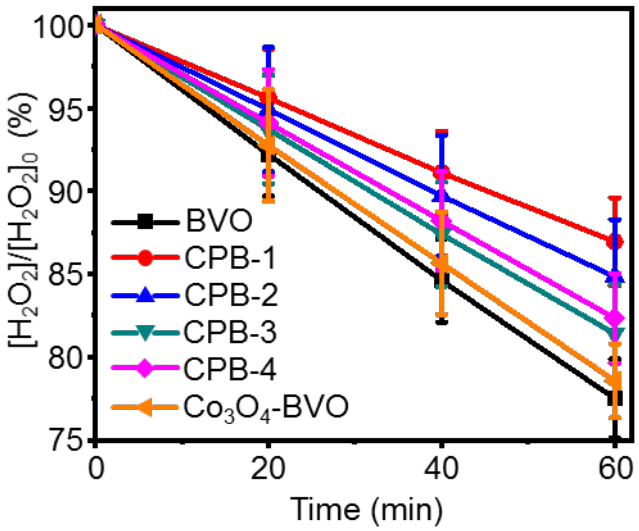

Figure S16. H_2O_2 desorption curves of BVO, CPB and Co_3O_4-BVO photoanodes with three times of independent experiments.

photoanodes for photoanodic H_2O_2 production			
photoanodes	**Electrolyte**	**Production rate (μmol min^{-1} cm^{-2})**	**References**
Co_3O_4/TiO_2	0.5 M $KHCO_3$	0.021 (1 mA at 0.4-1.2 V)	[1]
$WO_3/BiVO_4$	2 M $KHCO_3$	0.022 at 1.5 V *vs.* RHE	[2]
$WO_3/BiVO_4$	2 M $KHCO_3$	0.066 at 1.23 V *vs.* RHE	[3]
$BiVO_4$-Air/V	1 M $NaHCO_3$	0.092 at 1.23 V *vs.* RHE	[4]
CPB	1 M $KHCO_3$	0.16 at 1.7 V *vs.* RHE	This work

Table S1. Summary of reported photoanodes and this work for photoanodic H_2O_2 production.

References

[1] J. Zhang, X. Chang, Z. Luo, T. Wang, J. Gong, A highly efficient photoelectrochemical H_2O_2 production reaction with Co_3O_4 as a co-catalyst, Chem. Commun. 54 (2018) 7026-7029.

[2] K. Fuku, K. Sayama, Efficient oxidative hydrogen peroxide production and accumulation in photoelectrochemical water splitting using a tungsten trioxide/bismuth vanadate photoanode, Chem. Commun. 52 (2016) 5406-5409.

[3] K. Fuku, Y. Miyase, Y. Miseki, T. Funaki, T. Gunji, K. Sayama, Photoelectrochemical Hydrogen Peroxide Production from Water on a WO_3 /$BiVO_4$ Photoanode and from O_2 on an Au Cathode Without External Bias, Chem. Asian J. 12 (2017) 1111-1119.

[4] L. Wang, Y. Lu, N. Han, C. Dong, C. Lin, S. Lu, Y. Min, K. Zhang, Suppressing Water Dissociation via Control of Intrinsic Oxygen Defects for Awakening Solar H_2O-to-H_2O_2 Generation, Small 17 (2021) 2100400.